arXiv:1208.2229v1 [cond-mat.str-el] 10 Aug 2012

Magnetic structural change of Sr_2IrO_4 upon Mn doping

S. Calder,[1,*] G.-X. Cao,[2,3] M. D. Lumsden,[1] J. W. Kim,[4]
Z. Gai,[5] B. C. Sales,[3] D. Mandrus,[2,3] and A. D. Christianson[1]

[1]*Quantum Condensed Matter Division, Oak Ridge National Laboratory, Oak Ridge, TN 37831.*
[2]*Department of Materials Science and Engineering, University of Tennessee, Knoxville, TN 37996.*
[3]*Materials Science and Technology Division, Oak Ridge National Laboratory, Oak Ridge, TN 37831.*
[4]*Advanced Photon Source, Argonne National Laboratory, Argonne, IL 60439.*
[5]*Center for Nanophase Materials Sciences, Oak Ridge National Laboratory, Oak Ridge, TN 37830.*

(Dated: August 13, 2012)

The layered 5*d* transition metal oxide Sr_2IrO_4 has been shown to host a novel $J_{\rm eff}{=}\frac{1}{2}$ Mott spin orbit insulating state with antiferromagnetic ordering, leading to comparisons with the layered cuprates and consequently intriguing doping possibilities. Here we study the effect of substituting Mn for Ir in single crystals of $Sr_2Ir_{0.9}Mn_{0.1}O_4$. Through an investigation involving bulk measurements and resonant x-ray scattering we observe a new long range magnetic structure emerge upon doping with a reduction in the ordering temperature. The strong enhancement of the magnetic x-ray scattering intensity at the L_3 edge compared to the L_2 edge indicates that the $J_{\rm eff}{=}\frac{1}{2}$ state is robust and capable of hosting a variety of ground states.

The discovery of a novel spin-orbit coupling (SOC) driven state in Sr_2IrO_4 has focused attention on the possibility of further unique ground states emerging from the strong SOC found in the 5*d* transition metal oxides (TMO)[1]. In 5*d* TMOs the large radius of the electronic wavefunction and increased charge results in a delicate balance between reduced Coulomb interactions, increased SOC and crystal field splitting that are all of comparable strength (∼1 eV). Investigations of 5*d* systems have led to the realization of topological insulating states[2], Weyl semi-metal behavior[3], the Slater metal-insulator transition[4,5], unconventional superconductivity[6] and potentially the Kitaev model[7].

Sr_2IrO_4 was revealed to host a $J_{\rm eff}{=}\frac{1}{2}$ Mott spin orbit insulating state[1], that has subsequently been established to exist in the iridates $CaIrO_3$[8] and $Sr_3Ir_2O_7$[9,10]. The $J_{\rm eff}{=}\frac{1}{2}$ behavior arises from the *d*-manifold degeneracy, that is split by the crystalline electric field into the t_{2g} and e_g levels, being further broken by SOC driving the t_{2g} level into a lower energy $J_{\rm eff}{=}\frac{3}{2}$ degenerate quadruplet and a high energy $J_{\rm eff}{=}\frac{1}{2}$ degenerate doublet. For the $5d^5$ Ir^{4+} ion this results in a filled $J_{\rm eff}{=}\frac{3}{2}$ manifold and a half filled $J_{\rm eff}{=}\frac{1}{2}$ manifold that is split by even the small on-site Coulomb interactions in 5*d* TMOs. The similarity of the magnetic insulating state and the crystal structure in Sr_2IrO_4 with the layered cuprate La_2CuO_4 has led to interest in realizing superconductivity via doping Sr_2IrO_4[11,12]. Indeed an important open question is whether or not the $J_{\rm eff}{=}\frac{1}{2}$ state is robust to perturbations, such as doping, and consequently able to act as a vehicle from which unusual ground states can emerge.

Sr_2IrO_4 crystalizes into the tetragonal $I4_1/acd$ space group, shown in Fig. 1, with the IrO_6 octahedra rotated around the *c*-axis by ∼11°.[13,14] This results in the reduced symmetry of $I4_1/acd$ compared to $I4/mmm$. $Sr_2Ir_{0.9}Mn_{0.1}O_4$, the material of interest in this work, has Mn substituted on the Ir site that causes no symmetry change, as we confirmed by x-ray diffraction (XRD). For comparison a full series powder XRD investigation of $Sr_2Ir_{1-x}Ti_xO_4$ reported a change from $I4_1/acd$ to $I4/mmm$ for $x{\approx}0.4$, with a similar doping value inferred for Fe and Co[15]. The end member for our chosen doping, Sr_2MnO_4, indeed forms the $I4/mmm$ space group[16].

We present the first results of Mn-doped Sr_2IrO_4. Resonant x-ray scattering (RXS) has emerged as an important and powerful tool in the investigation of 5*d* magnetism, revealing the $J_{\rm eff}{=}\frac{1}{2}$ state in Sr_2IrO_4 and the long range magnetic structure[1]. We employ this technique to test the robustness of the $J_{\rm eff}{=}\frac{1}{2}$ state in Mn-doped Sr_2IrO_4 and to observe alterations to the magnetic structure. We report complimentary $Sr_2Ir_{0.9}Mn_{0.1}O_4$ single crystal measurements that consider changes in bulk magnetic correlations through magnetization and resistivity.

Single crystals of $Sr_2Ir_{0.9}Mn_{0.1}O_4$ were grown in a Pt crucible using the flux method. Measurements on a crystal of approximate size 1×1×0.5 mm was performed at the Advanced Photon Source (APS) at beamline 6-ID-B using magnetic RXS. We carried out measurements at both the L_2 (12.82 keV) and L_3 (11.22 keV) resonant edges of iridium. Graphite was used as the polarization analyzer at the (0 0 10) and (008) reflections on the L_2 and L_3 edges, respectively, to achieve a scattering angle close to 90°. Measurements were taken at several reflections to investigate possible magnetic structures, with an analysis of the photon polarization in σ-σ and σ-π allowing magnetic and charge scattering to be distinguished. To observe the sample fluorescence, energy scans were performed without the analyzer and with the detector away from any Bragg peaks through both absorption energies. The sample magnetization $M(T,H)$ was measured with a Quantum Design (QD) magnetic property measurement system (MPMS) in applied fields up to 7 T. The electrical resistivity $\rho(T,H)$ were performed using a QD 14T physical property measurement system (PPMS).

Undoped Sr_2IrO_4 forms a long-range AFM structure at 240 K with a net ferromagnetic moment arising from canting of the spins within the basal plane, with the de-

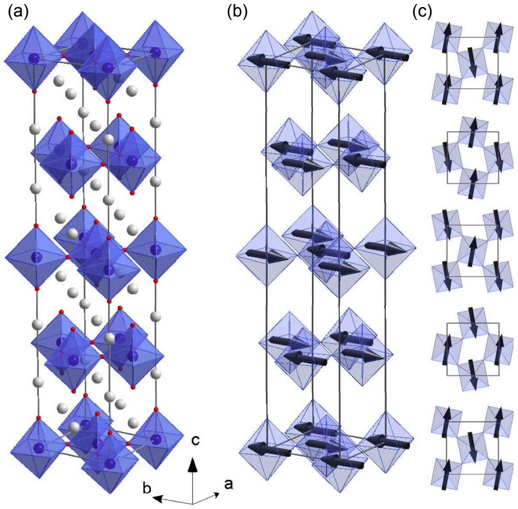

FIG. 1. (a) The crystal structure of $Sr_2Ir_{0.9}Mn_{0.1}O_4$ remains unchanged from Sr_2IrO_4, with space group $I4_1/acd$. Layers of $Ir_{0.9}Mn_{0.1}O_6$ octahedra are separated along the c-axis with a rotation of ∼11°. (b) Magnetic structure of Sr_2IrO_4 for H>0.2 T[1]. (c) The same magnetic ordering in each ab-plane in the unit cell is shown with the canting of the spins, following the rotation of the octahedra, producing a net ferromagnetic component. This magnetic structure, as well as other, symmetry-equivalent structures, have an ordering wave vector consistent with the observed magnetic scattering for $Sr_2Ir_{0.9}Mn_{0.1}O_4$.

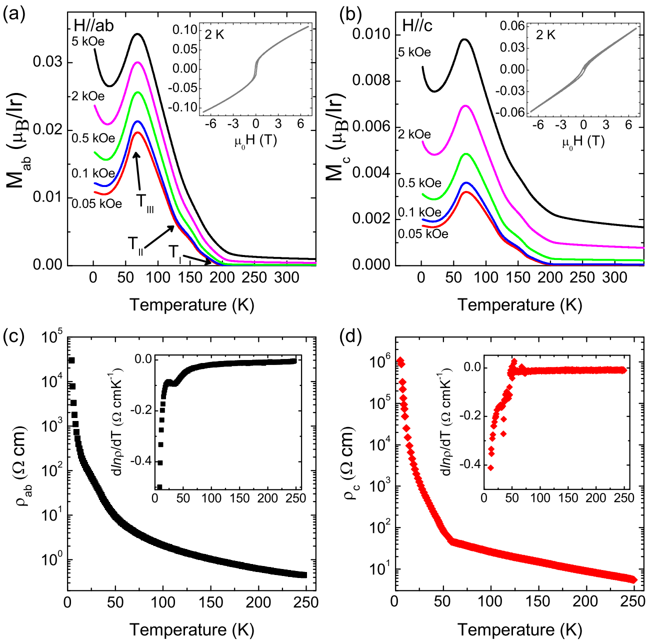

FIG. 2. Field cooled magnetization measurements on single crystals of $Sr_2Ir_{0.9}Mn_{0.1}O_4$ for applied fields parallel to the (a) ab-plane and (b) c-axis. Inset shows the isothermal magnetization from -7 to 7 T at 2 K. Zero field resistivity measurements along the (c) ab-plane and (d) c-axis.

gree of canting governed by the angle of rotation of the octahedra[1,17]. Magnetization results for $Sr_2Ir_{0.9}Mn_{0.1}O_4$ (Fig. 2(a)-(b)) show the onset of magnetic correlations occur around ∼170 K for low field cooled measurements, significantly reduced compared to Sr_2IrO_4. Increasing the applied field causes an increase in the transition temperature. The value of $0.11\mu_B$ at 2 K in the maximum field applied of 7 T (see Fig. 2(a) inset) is close to the saturated moment in the literature for Sr_2IrO_4 of $0.14\mu_B$[18]. The magnetization anisotropy between the c-axis and the ab-plane persists upon Mn-dopoing, with the ab-plane remaining as the easy axis. Discrete regions, separated by anomalies in the magnetization and resistivity, were evident in measurements for Sr_2IrO_4[19]. A similar distinction can be applied to $Sr_2Ir_{0.9}Mn_{0.1}O_4$ with anomalies in the magnetization at T_I=170 K, T_{II}=125 K and T_{III}∼55 K for the 0.05 kOe results, highlighted in Fig. 2(a). Increasing the applied field leads to a removal of the T_{II} anomaly. For Sr_2IrO_4 at low temperature (<20 K) the magnetization increased along the c-axis and decreased along the ab-plane, leading to the suggestion of increased canting of spins along the c-axis.[19] Figure 2(a)-(b), however, shows for $Sr_2Ir_{0.9}Mn_{0.1}O_4$ that M_{ab} and M_c both increase, indicating no enhanced c-axis canting.

In Sr_2IrO_4 the transition from a high temperature metallic phase to low temperature insulating state occurs without a well defined boundary above room temperature, with debate as to the possibility of a combination of Mott and magnetic correlations via the Slater mechanism driving the insulating state[20]. For $Sr_2Ir_{0.9}Mn_{0.1}O_4$ the resistivity remains unchanged through both T_I and T_{II}, see Fig. 2(c)-(d). The lack of a discernible change in the resistivity at the upper magnetic transitions indicates that the initial onset of magnetic order does not affect the electron scattering rate and therefore spin disorder scattering is not a significant term in the resistivity in this region. At T_{III}, however, concurrent with the sharp drop in the magnetization, the resistivity increases at a greater rate. The derivative of the resistivity shows this change to occur more clearly for both the c-axis and ab-plane, shown inset in Fig. 2(c)-(d). Therefore the T_{III} region shows a coupling of the magnetization and resistivity in three-dimensions, potentially due to a structural distortion or a change in the magnetic correlations that localizes the conduction electrons.

Having established 10% Mn-doping of Sr_2IrO_4 produces alterations in the magnetic correlations we consider the long range magnetic ordering. Given the high neutron absorption of Ir and low effective magnetic moment we performed a magnetic RXS measurement. As shown in Fig. 3(a)-(c) magnetic order for Ir ions is characterized by (1 0 odd) and (0 1 odd) reflections in $Sr_2Ir_{0.9}Mn_{0.1}O_4$. No magnetic scattering is observed at the (0 0 L), (1 1 L), ($\frac{1}{2}$ $\frac{1}{2}$ L) reflections or at incommensurate positions at 5, 80, 120, 160 or 170 K for the regions shown in Fig. 3(c). We note that the large charge reflections will obscure any potential magnetic scattering at (0 0 $4n$).

Figure 3(d) shows the temperature dependence of the

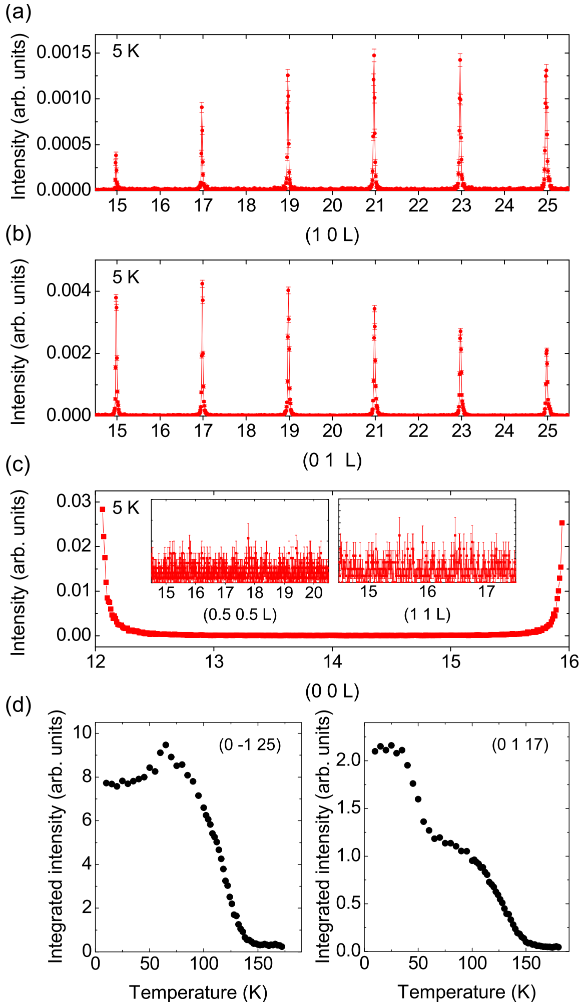

FIG. 3. Elastic RXS of $Sr_2Ir_{0.9}Mn_{0.1}O_4$ at the Ir L_3-edge in σ-π mode. (a)-(b) L scans at constant (H,K) reveal long range magnetic order at (1 0 *odd*) and (0 1 *odd*) at 5 K. The same reflections are present at 80 and 120 K. (c) No magnetic reflections are observed at (0 0 L), (1 1 L) or (0.5 0.5 L) positions at 5, 80, 120, 160 or 170 K. (d) The change in integrated intensity with temperature for two magnetic reflections.

integrated intensity for select magnetic peaks. The onset of long range magnetic order occurs at ~155 K. This is reduced compared to the applied-field magnetization results. This is, however, consistent with the observation that the application of even small fields causes an increase in the magnetic transition temperature in $Sr_2Ir_{0.9}Mn_{0.1}O_4$ and as such the zero field RXS should produce a lower T_N. To test for beam heating we compared the temperature dependence for an attenuator in the beam providing approximately a factor of 2 attenuation and no difference in the ordering temperature was observed. We cannot additionally rule out poor thermal contact or sample variation compounding this effect. Despite both chosen reflections showing the same magnetic ordering temperature, the lower temperature region around T_{III} showed anomalous behavior. To search for potential changes in the long range magnetic structure through this region we performed the same scans presented in Fig. 3(a)-(c) at various temperatures between 5 K and 170 K and observed no removal or development in the measured magnetic Bragg peaks. Therefore, although the long range magnetic structure remains unaltered, the region around T_{III} appears to host a change consistent with changes in the moment direction or a small structural distortion.

Comparing our results with RXS measurements on Sr_2IrO_4 demonstrates Mn doping forces an alteration to a new magnetic structure. Sr_2IrO_4 has magnetic scattering at (0 0 *odd*) as well as (1 0 4n+2) and (0 1 4n) reflections. The observation in Sr_2IrO_4 that (1 0 L) ≠ (0 1 L) requires a symmetry transition from tetragonal to orthorhombic[1]. Any potential departure from tetragonal is not observed within the resolution of our measurements for $Sr_2Ir_{0.9}Mn_{0.1}O_4$. The same study of Sr_2IrO_4 found an application of a small in-plane field of H > 0.2 T altered the magnetic structure such that the (1 0 4n+2) peaks disappear and new peaks appear at (1 0 *odd*) reflections. This allows us to speculate that Mn-doping of Sr_2IrO_4 simulates the behavior of Sr_2IrO_4 in a small magnetic field, with the in-field magnetic structure presented by Kim *et al.*[1] applicable to $Sr_2Ir_{0.9}Mn_{0.1}O_4$.

To explore the nature of the long range magnetic ordered structure we implemented representational analysis[21]. The propagation vector $\mathbf{k}$ = (0 0 0) was employed in our analysis as it is consistent with all the observed magnetic reflections. For a second order transition, Landau theory states that the symmetry properties of the magnetic structure are described by only one irreducible representation (IR). The space group $I4_1/acd$ and Ir ions on the 8a wyckoff position gives the IRs: Γ_1, Γ_3, Γ_6, Γ_8, Γ_9 and Γ_{10} (following the numbering scheme

TABLE I. BVs for space group $I4_1/acd$ with $\mathbf{k}$ = (0 0 0). The decomposition of the magnetic representation for the Ir^{4+} site is $\Gamma_{Mag} = 1\Gamma_1^1 + 0\Gamma_2^1 + 1\Gamma_3^1 + 0\Gamma_4^1 + 0\Gamma_5^1 + 1\Gamma_6^1 + 0\Gamma_7^1 + 1\Gamma_8^1 + 2\Gamma_9^2 + 2\Gamma_{10}^2$. The atoms of the nonprimitive basis are defined according to 1: (0 0 0), 2: (0 $\frac{1}{2}$ $\frac{3}{4}$), 3: (0 0 $\frac{1}{2}$), 4: (0 $\frac{1}{2}$ $\frac{1}{4}$).

IR	BV	Atom	BV components			IR	BV	Atom	BV components		
			$m_{\parallel a}$	$m_{\parallel b}$	$m_{\parallel c}$				$m_{\parallel a}$	$m_{\parallel b}$	$m_{\parallel c}$
Γ_9	ψ_5	1	1	0	0	Γ_{10}	ψ_9	1	1	0	0
		2	1	0	0			2	1	0	0
		3	1	0	0			3	-1	0	0
		4	1	0	0			4	-1	0	0
	ψ_6	1	0	1	0		ψ_{10}	1	0	1	0
		2	0	-1	0			2	0	-1	0
		3	0	-1	0			3	0	1	0
		4	0	1	0			4	0	-1	0
	ψ_7	1	0	-1	0		ψ_{11}	1	0	1	0
		2	0	-1	0			2	0	1	0
		3	0	-1	0			3	0	-1	0
		4	0	-1	0			4	0	-1	0
	ψ_8	1	1	0	0		ψ_{12}	1	-1	0	0
		2	-1	0	0			2	1	0	0
		3	-1	0	0			3	-1	0	0
		4	1	0	0			4	1	0	0

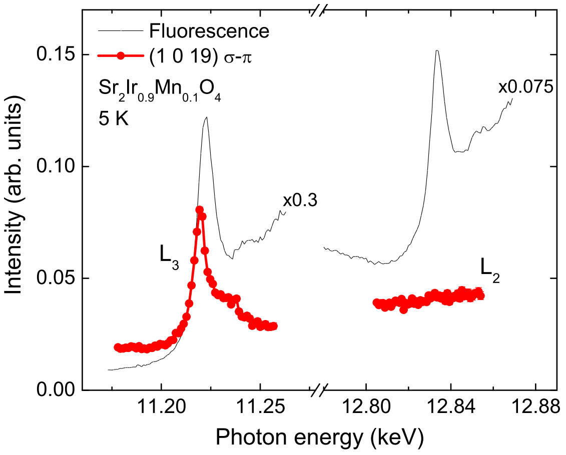

FIG. 4. RXS energy dependence of the iridium L$_3$-edge at 11.22 keV and the L$_2$-edge at 12.82 keV. These correspond to the inflection point at the low energy side of the enhancement in the fluorescence scans. Measurements at both edges of $Sr_2Ir_{0.9}Mn_{0.1}O_4$ only yields appreciable resonant enhancement at the L$_3$ edge for σ-π magnetic scattering. This behavior is a signature of $J_{\mathrm{eff}}=\frac{1}{2}$ state.

of Kovalev[22]). Γ_1, Γ_3, Γ_6 and Γ_8 only have moments parallel to the c-axis. We exclude these due to the magnetic structure of undoped Sr_2IrO_4 that has spins confined to the ab-plane[1] and consider the introduction of Mn on the Ir site as a perturbation on the undoped magnetic structure. This is supported by the similar magnetization results for undoped and Mn-doped Sr_2IrO_4 that has the ab-plane as the easy axis and the unchanged crystal structure that promotes magnetization in the ab-plane.[17]

For the two remaining IRs, listed in Table I, only Γ_9 with basis vectors (BVs) ψ_6 and ψ_8 and Γ_{10} with BVs ψ_9 and ψ_{11} give scattering at the experimentally observed magnetic reflections. The magnetic structure produced by each of the separate BVs can be transformed into the magnetic structure given by another BV with the reversal of either $c \rightarrow -c$ or $a \rightarrow b$. The only distinction is the predicted intensities at various (1 0 *odd*) and (0 1 *odd*) positions. Given the different absorption effects in different crystallographic orientations in the RXS measurements coupled with the unpredictable effects of multiple scattering we cannot faithfully assign an unambiguous ordering of the magnetic structure in the ab-plane. While these BVs produce the correct experimental AFM scattering, they do not account for the net FM moment observed in magnetization measurements. The remaining BVs, ψ_5 and ψ_7 for Γ_9 and ψ_{10} and ψ_{12} for Γ_{10}, produce FM ordering within the ab-layers. Therefore to produce the observed magnetic behavior for $Sr_2Ir_{0.9}Mn_{0.1}O_4$ requires a combination of AFM and FM BVs. For Γ_9 a linear combination of the BVs $c_1\psi_6 + c_2\psi_5$, where the coefficient c_1 controls the AFM moment and c_2 the degree of canting via the FM moment, gives the the magnetic structure presented by Kim *et al.* in a 0.3 T magnetic field[1]. We therefore present this as a potential magnetic structure for $Sr_2Ir_{0.9}Mn_{0.1}O_4$, shown schematically in Fig. 1(b)-(c). As such the long range magnetic structure with a net magnetic moment comes out naturally from our representational analysis, with the canting of the moments dictated by the orientation of the octahedra[17]. The observation that 10% Mn substitution for Ir or a small field of 0.2 T alters the long range magnetic structure in a similar fashion allows us to advance two points. Firstly that the introduced Mn ions mimic the behavior of a magnetic field and are therefore magnetic in $Sr_2Ir_{0.9}Mn_{0.1}O_4$. Secondly it suggests that the magnetic ordered state in Sr_2IrO_4 is potentially unstable and can be influenced by other perturbations. This observation is encouraging with regards to the search for superconductivity.

The resonant enhancement for Ir not only allows RXS to be utilized to observe long range magnetic ordering, but gives a signature of the $J_{\mathrm{eff}}=\frac{1}{2}$ Mott insulating state[1]. In a non-SOC split Ir^{4+} t_{2g} manifold a large enhancement is expected at both L_2 and L_3 edges, however the scattering at L_2 is forbidden for the $J_{\mathrm{eff}}=\frac{1}{2}$ SOC induced state. Therefore a measurement of the intensity through the resonant energies at allowed magnetic reflections provides direct evidence for the existence of the $J_{\mathrm{eff}}=\frac{1}{2}$ state. Such measurements are presented in Fig. 4 at the (1 0 19) magnetic reflection. A large enhancement is observed at the L_3 edge that has its maximum at the inflection point of the fluorescence scans, as expected. Conversely there is no appreciable resonant enhancement at the L_2 energy. The $J_{\mathrm{eff}}=\frac{1}{2}$ state remains in $Sr_2Ir_{0.9}Mn_{0.1}O_4$, despite the change in magnetic structure. The $J_{\mathrm{eff}}=\frac{1}{2}$ state has been shown to exist in iridates other than Sr_2IrO_4, that host alternative crystal symmetries[8–10], and now upon diluting the Ir site with a 3d magnetic ion that has reduced SOC and cannot itself host the state. This points to the robustness of the $J_{\mathrm{eff}}=\frac{1}{2}$ state despite the apparent ease of altering the magnetic structure it inhabits. It would be of interest to follow Mn-doped Sr_2IrO_4, or an alternative doping, through the expected $I4_1/acd$ to $I4/mmm$ doping driven structural transition. Such a structural change would be expected to lead to a spin-flop transition[10,17], however it is not clear whether the robustness of the $J_{\mathrm{eff}}=\frac{1}{2}$ state, or indeed long range magnetic order, would be maintained upon such high dilution of Ir sites.

Our results show that substituting Mn for Ir in Sr_2IrO_4 leads to an alteration of the magnetic structure, with the onset of magnetic ordering reduced from 240 K to ∼155 K and controllable by applied fields. Even with the altered long range magnetic ordering of the Ir ions the $J_{\mathrm{eff}}=\frac{1}{2}$ insulating state remains. The effect of 10% Mn doping is consistent with the application of a small field of 0.2 T to Sr_2IrO_4. Despite speculation as to the possibilities of doping Sr_2IrO_4, few experimental studies exist. The results presented suggest an unstable magnetic structure in Sr_2IrO_4 that can be altered by small perturbations, whereas breaking the $J_{\mathrm{eff}}=\frac{1}{2}$ state appears to require a more dramatic alteration. Further studies using alternative doping ions and concentrations will lead to a greater level of understanding in this important 5d material.

We thank Ling Li for supporting characterization measurements. Work at ORNL, including a portion of this research at the Center for Nanophase Materials Sciences, was supported by the scientific User Facilities Division, Office of Basic Energy Sciences, U.S. Department of Energy (DOE) and Materials Sciences and Engineering Division, Office of Science, U.S. DOE. Use of the Advanced Photon Source, an Office of Science User Facility operated for the U.S. DOE Office of Science by Argonne National Laboratory, was supported by the U.S. DOE under Contract No. DE-AC02-06CH11357.

---

* caldersa@ornl.gov

[1] B. J. Kim, H. Ohsumi, T. Komesu, S. Sakai, T. Morita, H. Takagi, and T. Arima, Science, **323**, 1329 (2009).

[2] D. Pesin and L. Balents, Nature Phys., **6**, 376 (2010).

[3] X. Wan, A. M. Turner, A. Vishwanath, and S. Y. Savrasov, Phys. Rev. B, **83**, 205101 (2011).

[4] S. Calder, V. O. Garlea, D. F. McMorrow, M. D. Lumsden, M. B. Stone, J. C. Lang, J.-W. Kim, J. A. Schlueter, Y. G. Shi, K. Yamaura, Y. S. Sun, Y. Tsujimoto, and A. D. Christianson, Phys. Rev. Lett., **108**, 257209 (2012).

[5] Y. G. Shi, Y. F. Guo, S. Yu, M. Arai, A. A. Belik, A. Sato, K. Yamaura, E. Takayama-Muromachi, H. F. Tian, H. X. Yang, J. Q. Li, T. Varga, J. F. Mitchell, and S. Okamoto, Phys. Rev. B, **80**, 161104 (2009).

[6] S. Yonezawa, Y. Muraoka, Y. Matsushita, and Z. Hiroi, J. Phys.: Cond. Matt., **16**, L9 (2004).

[7] J. c. v. Chaloupka, G. Jackeli, and G. Khaliullin, Phys. Rev. Lett., **105**, 027204 (2010).

[8] N. A. Bogdanov, V. M. Katukuri, H. Stoll, J. van den Brink, and L. Hozoi, Phys. Rev. B, **85**, 235147 (2012).

[9] J. W. Kim, Y. Choi, J. Kim, J. F. Mitchell, G. Jackeli, M. Daghofer, J. van den Brink, G. Khaliullin, and B. J. Kim, Phys. Rev. Lett., **109**, 037204 (2012).

[10] S. Boseggia, R. Springell, H. C. Walker, A. T. Boothroyd, D. Prabhakaran, D. Wermeille, L. Bouchenoire, S. P. Collins, and D. F. McMorrow, Phys. Rev. B, **85**, 184432 (2012).

[11] J. Kim, D. Casa, M. H. Upton, T. Gog, Y.-J. Kim, J. F. Mitchell, M. van Veenendaal, M. Daghofer, J. van den Brink, G. Khaliullin, and B. J. Kim, Phys. Rev. Lett., **108**, 177003 (2012).

[12] F. Wang and T. Senthil, Phys. Rev. Lett., **106**, 136402 (2011).

[13] M. K. Crawford, M. A. Subramanian, R. L. Harlow, J. A. Fernandez-Baca, Z. R. Wang, and D. C. Johnston, Phys. Rev. B, **49**, 9198 (1994).

[14] Q. Huang, J. Soubeyroux, O. Chmaissem, I. Sora, A. Santoro, R. Cava, J. Krajewski, and W. P. Jr., Journal of Solid State Chemistry, **112**, 355 (1994), ISSN 0022-4596.

[15] A. J. Gatimu, R. Berthelot, S. Muir, A. W. Sleight, and M. Subramanian, Journal of Solid State Chemistry, **190**, 257 (2012), ISSN 0022-4596.

[16] K. Tezuka, M. Inamura, Y. Hinatsu, Y. Shimojo, and Y. Morii, Journal of Solid State Chemistry, **145**, 705 (1999), ISSN 0022-4596.

[17] G. Jackeli and G. Khaliullin, Phys. Rev. Lett., **102**, 017205 (2009).

[18] G. Cao, J. Bolivar, S. McCall, J. E. Crow, and R. P. Guertin, Phys. Rev. B, **57**, R11039 (1998).

[19] M. Ge, T. F. Qi, O. B. Korneta, D. E. De Long, P. Schlottmann, W. P. Crummett, and G. Cao, Phys. Rev. B, **84**, 100402 (2011).

[20] R. Arita, J. Kuneš, A. V. Kozhevnikov, A. G. Eguiluz, and M. Imada, Phys. Rev. Lett., **108**, 086403 (2012).

[21] A. Wills, Physica B, **276**, 680 (2000).

[22] O. V. Kovalev, *Representations of the Crystallographic Space Groups Edition 2* (Gordon and Breach Science Publishers, Switzerland, 1993).